EPJ A
Hadrons and Nuclei

EPJ.org
your physics journal

Eur. Phys. J. A (2017) **53**: 67 DOI 10.1140/epja/i2017-12259-8

On possible shape isomers in the Pt-Ra region of nuclei

B. Nerlo-Pomorska, K. Pomorski, J. Bartel and C. Schmitt

Società Italiana di Fisica

Springer

Eur. Phys. J. A (2017) **53**: 67
DOI 10.1140/epja/i2017-12259-8

THE EUROPEAN PHYSICAL JOURNAL A

Regular Article – Theoretical Physics

On possible shape isomers in the Pt-Ra region of nuclei

B. Nerlo-Pomorska[1], K. Pomorski[1,a], J. Bartel[2], and C. Schmitt[2,3]

[1] UMCS, Lublin, Poland
[2] IPHC, Strasbourg, France
[3] GANIL, Caen, France

Received: 28 December 2016 / Revised: 13 March 2017
Published online: 11 April 2017

Communicated by T. Duguet

Abstract. A certain number of yet unknown super- and hyper-deformed shape isomeric states are predicted in even-even nuclei of the region between Pt and Ra, using the macroscopic-microscopic model based on the Lublin Strasbourg Drop for the macroscopic energy and shell plus pairing corrections evaluated through the Yukawa-folded mean-field potential for the microscopic part. A new, rapidly converging shape parametrization is used to describe the vast range of nuclear deformations between the ground and the fission isomeric states up to near the scission configuration. Quadrupole moments are evaluated in the local minima and turn out to be in good agreement with the experimental data wherever available.

1 Introduction

The first shape isomer ^{242m}Am was discovered in 1962 by Polikanov *et al.* [1] in the ^{242}Pu(d, 2n)^{242}Am reaction. They observed an activity with a very short half-life of the order of ms. The first theoretical interpretation of this discovery as super-deformed (sd) shape isomer with the main axis ratio 1:2 was proposed by Strutinsky [2] who showed that taking into account the shell energy leads to the appearance of a second minimum in the fission barrier. Until that time one assumed that the shell-correction effects could generate the ground state deformation only and that they disappeared with growing nuclear deformation, and that the region of the fission barrier saddle was determined by the liquid-drop model [3]. The Polikanov discovery and its attractive interpretation given by Strutinsky has initiated both experimental and theoretical research in this field. Already in the next decade one discovered 33 super-deformed shape isomers in the actinide region. The analysis of the transmission probability of resonances in prompt fission induced by γ or light particles has suggested the existence of even more deformed isomeric states called hyper-deformed (hd). Such third minima were discovered in $^{230-233}$Th [4–9], ^{232,234,236}U, and ^{232}Pa nuclei [10–13].

Theoretical predictions of the ground state and shape isomeric minima as well as the saddle-point energies obtained for more than 7000 isotopes with $A \geq 31$ within the macroscopic-microscopic model are presented in ref. [14]. They were based on extended macroscopic-microscopic calculations in a three-dimensional (3D) deformation-parameter space using the Nillson quadrupole axial (ε_2), nonaxial (γ), and hexadecapole (ε_4) deformation parameters. The finite-range liquid-drop model (FRLDM) was used in ref. [14] for the macroscopic part of the energy while the Yukawa-folded single-particle potential [15] for the microscopic part. The range of deformations used to perform the calculations was sufficient for locating the super-deformed isomers, but not the very elongated (hyper-deformed) shapes for which the use of higher multipolarities was necessary. The macroscopic-microscopic model of ref. [14] was extended in ref. [16] to 5 dimensions for nuclei with charge and mass numbers in the range $88 \leq Z \leq 94$ and $230 \leq A \leq 236$. In the barriers of the nuclei from this mass region only a few were found with third minima for light Th and U isotopes, which, however, turned out to be less than 1 MeV deep.

Similar extended studies of possible third hyper-deformed minima in even-even Th, U, and Pu nuclei were performed by Kowal and Skalski [17]. They made calculations in a 8D space spanned by the β_λ ($\lambda = 1, 2, \ldots, 8$) deformation parameters (in a spherical harmonics expansion). The Yukawa plus exponential model [18], and in parallel, the Lublin Strasbourg version of the liquid drop (LSD) [19], were used to evaluate the macroscopic part of the nuclear energy while the Woods-Saxon single-particle levels were used to obtain the microscopic energy correc-

[a] e-mail: pomorski@kft.umcs.lublin.pl

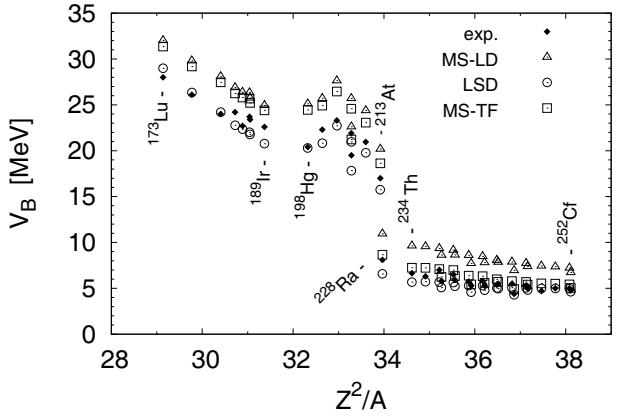

Fig. 1. Fission barrier heights obtained using the Myers-Świątecki liquid drop (MS-LD, triangles) [3], the Lublin Strasbourg Drop (LSD, circles) [19], the Myers and Swiatecki Thomas-Fermi model (MS-TH, squares) [35], and the experimental data (exp., dots) taken from the table in ref. [35] as a function of Z^2/A.

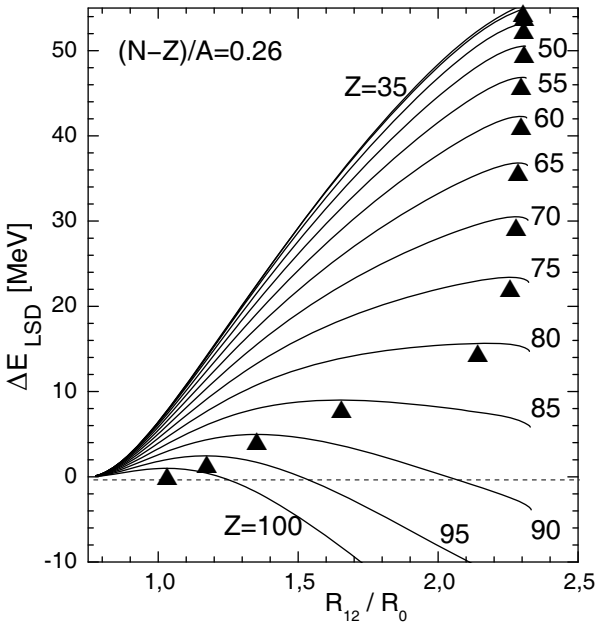

Fig. 2. LSD fission barrier profiles obtained for different charge numbers Z and a relative neutron excess $(N-Z)/A = 0.26$ using the optimal (*i.e.*, deformation-parameterless approach) shape Strutinsky theory [36] as a function of the relative distance between the mass centres of the nascent fragments in symmetric fission.

tions. It was shown in this 8D calculation that the third minima predicted in the $^{230-232}$Th isotopes are much less deep (< 0.5 MeV) than in previous theoretical estimates (3–4 MeV) (*e.g.*, in ref. [20]).

Also several attempts to find very exotic deformed configurations in the actinide region were undertaken using self-consistent models. One should mention here the HFB calculations made with the Gogny force [21,22], or the HF+BCS results obtained in ref. [23] using the SkM* Skyrme force [24]. Using the SkM* force and the UNEDF1 the Potential Energy Surfaces (PESs) in Th and U isotopes were studied in ref. [25]. No, or only very shallow third minima were found in the PES of ^{232}Th and ^{232}U, whereas these minima appeared deeper for the more neutron-deficient Th and U nuclei with neutron number $N = 136$ and 138.

A new interest in the fission barrier particularities of nuclei lighter than the actinides was triggered by the experiment of Andreyev *et al.* [26] who discovered an asymmetric fission in the ^{180}Hg isotope. Several calculations of the PES of nuclei in this region where performed [27–33]. The majority of these theoretical papers concentrated only on an explanation of a before unexpected asymmetric mass distribution of the fission fragments but not on the properties of local minima visible in the PES at very elongated nuclear shapes.

In the present paper we are going to concentrate on properties of the super- and hyper-deformed shape isomers in the preactinide even-even nuclei. We have chosen the LSD model for the macroscopic part of the nuclear energy as it very well reproduces the measured fission barrier heights (V_B) in a wide mass region of the nuclear chart as can be seen in fig. 1. The theoretical fission barrier heights presented in fig. 1 were evaluated in ref. [34] on the basis of the *topographical theorem* of Świątecki [35], *i.e.* as a difference between the macroscopic saddle-point and the experimental ground state masses. The nuclei of our present study correspond to $32 \leq Z^2/A \leq 34$.

The LSD fission barriers evaluated for several charge numbers $35 \leq Z \leq 100$ with a relative neutron excess $(N-Z)/A = 0.26$ are shown in fig. 2 as a function of the relative distance between the nascent fission-fragment mass centres (R_{12}). The optimal-shape theory of Strutinsky [36] was used to evaluate the barrier profiles. All evaluated fission barriers end at the geometrical scission point (two touching fragments). Saddle points are marked by triangles. It is seen in fig. 2 that with decreasing charge number the liquid-drop barrier heights grow, which is rather well known, and the saddle points are shifted towards larger elongations which for $Z \leq 70$ almost coincide with the scission point. It is also seen that for $Z < 90$ the LSD energy corresponding to the scission configuration is higher than the LSD energy of the spherical nucleus, which prevents the spontaneous fission of such nuclei. The very broad and flat liquid-drop fission barriers of pre-actinide nuclei ($Z \lesssim 85$) indicate that the inclusion of shell effects will have a good chance to produce local minima in the PES, corresponding to super- or/and hyper-deformed shapes. Extended calculations for long isotopic chains of even-even nuclei from platinium ($Z = 78$) to radium ($Z = 88$) have therefore been performed in the present paper within the macroscopic-microscopic model. A new rapidly convergent shape parametrization developed in ref. [37] was used to describe the shapes of a deformed nucleus from its ground state up to near the scission configuration.

2 Macroscopic-microscopic model and shape parametrization

The nuclear deformation energies of our analysis were determined in the macroscopic-microscopic model

$$E_{\rm tot}(Z,A;{\rm def}) = E_{\rm macr}(Z,A;{\rm def}) + E_{\rm micr}(Z,A;{\rm def}). \tag{1}$$

The Lublin Strasbourg Drop (LSD) model [19] has been used for the macroscopic part ($E_{\rm macr}$) of the potential-energy surface. The microscopic effects ($E_{\rm micr}$) have been evaluated through a Yukawa-folded (YF) single-particle potential [15] with the parameters listed in ref. [38], where also our way of solving of the eigenproblem of the YF Hamiltonian is described. Eighteen deformed harmonic oscillator shells were taken into account when diagonalising the YF Hamiltonian.

The Strutinsky shell-correction method [2,39] with an 8th-order correctional polynomial and a smearing width $\gamma_S = 1.2\,\hbar\omega_0$, where $\hbar\omega_0 = 41/A^{1/3}\,$MeV is the spherical harmonic-oscillator frequency, is used. The BCS [40] theory, including an approximate GCM+GOA particle-number projection as described in refs. [41,42] was used for the pairing correlations. The pairing strength equal to $G\cdot\mathcal{N}^{2/3} = 0.28\,\hbar\omega_0$, (with $\mathcal{N} = Z, N$ for proton or neutron, respectively) was adjusted to the experimental mass differences of nuclei in this region using a pairing window composed of $2\sqrt{15\mathcal{N}}$ single-particle levels closest to the Fermi surface.

A new nuclear shape parametrization [37,33] is used that gives an expansion of the nuclear surface in the form of a Fourier analysis in cylindrical coordinates

$$\frac{\rho_s^2(z)}{R_0^2} = \sum_{n=1}^{\infty}\left[a_{2n}\cos\left(\frac{(2n-1)\pi}{2}\,\frac{z-z_{\rm sh}}{z_0}\right) + a_{2n+1}\sin\left(\frac{2n\pi}{2}\,\frac{z-z_{\rm sh}}{z_0}\right)\right], \tag{2}$$

where, similarly to the famous "Funny-Hills" (FH) shape parametrization [39], $\rho_s(z)$ defines the distance of the equivalent sharp surface from the symmetry z-axis, and z_0 is half the elongation of the nuclear shape along that axis with end points located at $z_{\rm min} = z_{\rm sh} - z_0$ and $z_{\rm max} = z_{\rm sh} + z_0$. The coordinate $z_{\rm sh}$ is chosen so as to locate the centre of mass of the shape at the origin of the coordinate system. R_0 represents the radius of the corresponding spherical shape having the same volume and $z_0 = c\,R_0$ makes the connection with the FH elongation parameter c which can be expressed through the even (left-right symmetric) Fourier coefficients by the relation

$$\frac{\pi}{3c} = \sum_{n=1}^{\infty}(-1)^{n-1}\,\frac{a_{2n}}{2n-1}\,. \tag{3}$$

The parameters a_2, a_3, a_4 are related to quadrupole, octupole, and hexadecapole deformations, which in the context of fission, represent the elongation, left-right asymmetry, and neck degree of freedom, respectively. One should note that a spherical shape corresponds to a value of $a_2^{(0)}$ close to unity, with almost vanishing higher-order even $a_n^{(0)}$ parameters

$$a_2^{(0)} = 1.03205, \quad a_4^{(0)} = -0.03822, \quad a_6^{(0)} = 0.00826, \cdots. \tag{4}$$

More and more elongated prolate shapes correspond to decreasing values of a_2, while oblate ones are described by a_2 larger than one, which is somehow contrary to the traditional definition of a quadrupole deformation parameter. We will show below, how to obtain a more *natural* definition of that quadrupole deformation parameter.

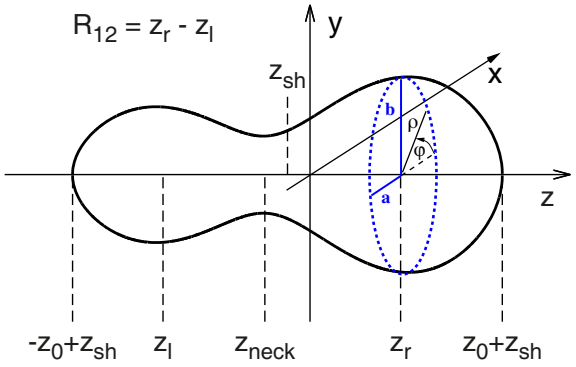

Fig. 3. (Color online) Schematic visualization in cylindrical coordinates of the parameters entering the definition of the profile function defined with eqs. (2)–(6). The quantities $z_{\rm l}$ and $z_{\rm r}$ localize the mass centres of the left and right nascent fragments entering the definition of R_{12}.

To account for the possibility of non-axial nuclear shapes, the profile function can be factorized as [43–45]

$$\varrho_s^2(z,\varphi) = \rho_s^2(z)\,\frac{1-\eta^2}{1+\eta^2+2\eta\cos(2\varphi)}\,, \tag{5}$$

where $\rho_s^2(z)$ is given by eq. (2) and φ is the usual azimuthal angle in cylindrical coordinates (see fig. 3). The non-axiality parameter η appearing in eq. (5) is the relative difference of the half axis of the cross section perpendicular to the z-axis, assumed here to be of ellipsoidal form,

$$\eta = \frac{b-a}{b+a}\,, \tag{6}$$

where the condition $a\,b = \rho_s^2$ ensures volume conservation for a non-axially deformed shape. This definition, together with the expressions for the semi-axis

$$a(z) = \rho_s(z)\,\sqrt{\frac{1-\eta}{1+\eta}} \quad \text{and} \quad b(z) = \rho_s(z)\,\sqrt{\frac{1+\eta}{1-\eta}}\,, \tag{7}$$

guarantees that η is independent of z. The description can be extended to a z-dependent η, and non-ellipsoidal cross sections, which might lead to energetically more favourable configurations when approaching the scission line. For simplicity we are, however, keeping the present description with a z-independent η value.

The different quantities entering eqs. (2)–(7) can be visualized in fig. 3, where the distance R_{12} between the

centres of mass of the left and right nascent fragment has been introduced as a measure for the elongation of the shape (see ref. [33] for details).

Let us come back for a moment to axially symmetric shapes and study the convergence of the Fourier series, eq. (2). To that purpose we have drawn in fig. 4 the relative importance of the contributions of the different Fourier terms for a well deformed left-right asymmetric shape. It immediately becomes clear that beyond $k = 4$ (here $k = 2n$ or $2n - 1$, see eq. (2)) the contribution from higher multipolarities turns out to be very small, even for such a strongly deformed shape as considered here. That indicates already at this stage, that one should be able to describe the very large variety of nuclear shapes between the ground state up to very large deformations close to the scission instability, where the nucleus splits into two fission fragments, with only 4 deformation parameters corresponding respectively to elongation, left-right asymmetry, neck degrees of freedom and non-axiality. Starting from the non-axiality parameter η of eqs. (5)–(7) plus the corresponding 3 Fourier deformation parameters a_2, a_3, a_4, we are therefore defining 4 collective coordinates q_1, q_2, q_3, q_4 which will also help us to cure the above mentioned *unnatural* behaviour of the quadrupole parameter a_2. What we aim at, is to define these q_n, for a very large variety of nuclei, in such a way that along the LD fission path these parameters show only a small variation around zero. We will show below that this aim is achieved by the following definitions

$$
\begin{aligned}
q_2 &= \frac{a_2^{(0)}}{a_2} - \frac{a_2}{a_2^{(0)}}\,, \qquad q_3 = a_3,\\
q_4 &= a_4 + \sqrt{\left(\frac{q_2}{9}\right)^2 + \left(a_4^{(0)}\right)^2}\,,\\
q_5 &= a_5 - (q_2 - 2)\,\frac{a_3}{10}\,,\\
q_6 &= a_6 - \sqrt{\left(\frac{q_2}{100}\right)^2 + \left(a_6^{(0)}\right)^2}\,,
\end{aligned}
\tag{8}
$$

where, as in (4), $a_n^{(0)}$ stands for the value of the a_n coefficient in the spherically symmetric case. It becomes immediately evident from (8) that the spherical case is described by $q_2 = 0$, while prolate deformations correspond to $q_2 > 0$ and oblate shapes to $q_2 < 0$.

The deformation-energy landscapes that we are going to discuss in the next section are thus described by 4 deformation parameters $q_1 = \eta$ (non-axiality) and q_2, q_3, q_4, while q_5 and q_6 (and higher-order terms) are set to zero, which, however, implies non-zero values of the corresponding a_5 and a_6 coefficients. That the above definitions, eq. (8) are, indeed, meaningful is demonstrated in fig. 5, which shows different sections of the LD deformation-energy landscape. The fact that the LD path to fission for a nuclear system with fissility parameter $x = 0.8$ in fig. 5 goes along $q_3 = q_4 = q_5 = q_6 = 0$ shows that the above definitions of the q_n parameters really make sense and are, at this stage, the best we can do, having no handle on the quantum corrections that come into play through the shell and pairing energies. Since the q_n parameters are

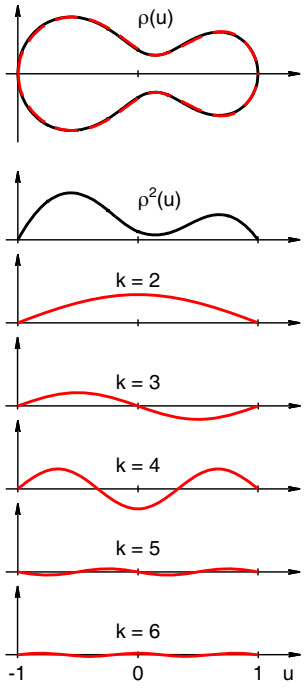

Fig. 4. (Color online) Relative importance of the contributions to the shape function $\rho_s^2(z)$, eq. (2), corresponding to different multipole orders of the Fourier series, for a left-right asymmetric shape displayed in the top part of the figure. Shapes are plotted as a function of the reduced variable $u = (z - z_{\rm sh})/z_0$.

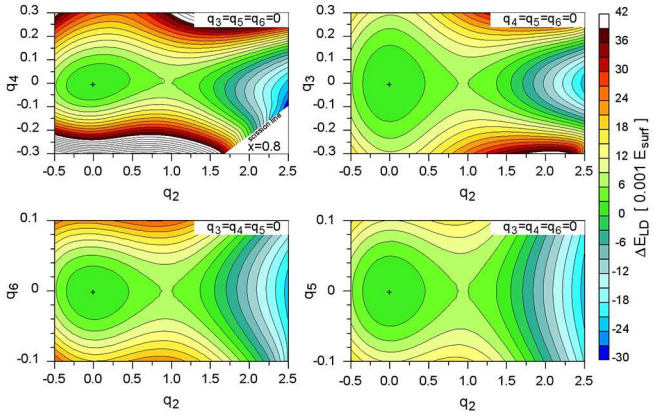

Fig. 5. (Color online) LD potential energy in the (q_2, q_4) (top left), (q_2, q_3) (top right), (q_2, q_6) (bottom left) and (q_5, q_2) (bottom right) deformation sub-spaces for a nucleus with fissility $x = 0.8$. In each (q_i, q_j) plot, the collective coordinates q_k with $k \neq i, j$ are set to zero.

defined as simple combinations of the a_n, where the latter constitute an orthogonal basis, the q_n, as the a_n, represent independent deformation variables.

Thanks the fast convergence of the Fourier series, we therefore believe that the above defined 4 deformation parameters q_1 to q_4 (with $q_5 = q_6 = 0$) are sufficient to describe the large variety of nuclear shapes up to very large deformations and we have thus been able to identify several shape isomers in our calculations. The deformation

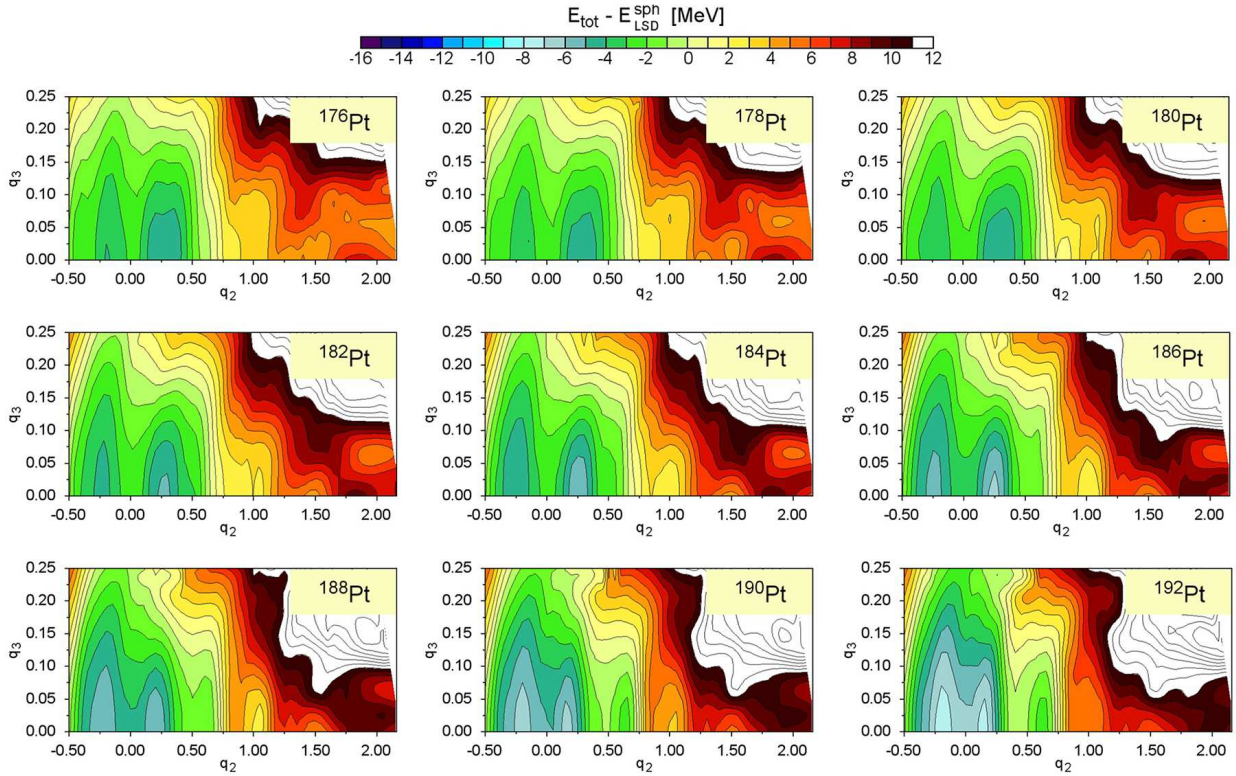

Fig. 6. Potential-energy surfaces (relative to the spherical LSD energy) for Pt isotopes in the (q_2, q_3) plane. All energies are minimised with respect to η (non-axial mode) and q_4 (neck mode).

energies and quadrupole moments of the most pronounced minima have also been evaluated, and are presented below.

3 Deformation energies

Nuclear deformation-energy landscapes (relative to the corresponding spherical LD energy) were calculated for even-even nuclei of different isotopic chains, $^{176-192}$Pt, $^{178-194}$Hg, $^{180-208}$Pb, $^{194-210}$Po, $^{196-212}$Rn and $^{208-236}$Ra in the pre-actinide region between platinum ($Z = 78$) and radium ($Z = 88$). They are presented in figs. 6 to 12 in the (q_2, q_3) plane, corresponding, as explained above, to the elongation and reflection asymmetry coordinates. In all these calculations a minimization with respect to the non-axiality and the neck degrees of freedom (parameters q_1 and q_4) was carried out at each deformation point. A similar analysis of some selected isotopes from the actinide region from Th to U was already performed in [46–48], and we will include some of the results of that investigation in our discussion below, since they help to give a more complete picture of that whole mass region.

It is interesting to analyse the different super- and hyper-deformed local minima that appear in the PES of nuclei from this region. Such minima, when deep enough (around 1 MeV or deeper) can lead to shape isomers similar to those observed for heavier nuclei of that mass region.

Starting with the Pt isotopes shown in fig. 6, we observe two energy minima: one oblate ($q_2 \approx -0.2$) and one deeper prolate ($q_2 \approx 0.3$). Beyond ^{184}Pt they become comparable in energy and also get closer to each other, tending towards an almost spherical shape ($|q_2| \approx 0.15$) for ^{192}Pt. All ground state (gs) minima are found to be left-right symmetric ($q_3 = 0$). The super-deformed (sd) and hyper-deformed (hd) minima, that turn out to be rather shallow for the lightest Pt nuclei, but become more pronounced for the heavier isotopes are observed around $q_2 \approx 1$ and $q_2 \approx 1.5$, respectively. Starting with ^{188}Pt and all the way up to ^{192}Pt one can identify an additional local minimum appearing around $q_2 \approx 0.6$ the depth of which grows with increasing neutron number. In ^{192}Pt the sd minimum around $q_2 = 1$ has practically disappeared while the minimum at $q_2 \approx 0.6$, is well identified. The above local minima correspond all to axially symmetric shapes. One also observes that in all investigated Pt isotopes an asymmetric fission valley is formed at elongations $q_2 \geq 1.7$.

The situation is slightly different for the Hg isotopic chain as presented in fig. 7. The lightest Hg isotope, ^{178}Hg, is practically spherical with a very flat potential energy with respect to quadrupole q_2 deformation. Its super-deformed minimum at $q_2 \approx 1$ corresponds to a pear-like shape ($q_3 \neq 0$) and is around 2 MeV deep. The hyper-deformed minimum at $q_2 \approx 1.5$ is also slightly left-right asymmetric, but its depth is only of about 1 MeV. With growing mass number, the left-right asymmetry of both the sd and hd shape isomers becomes smaller and smaller. The best candidates for sd Hg isomers are isotopes with $A = 178$–182 and 188–194. In the heaviest Hg nuclei the

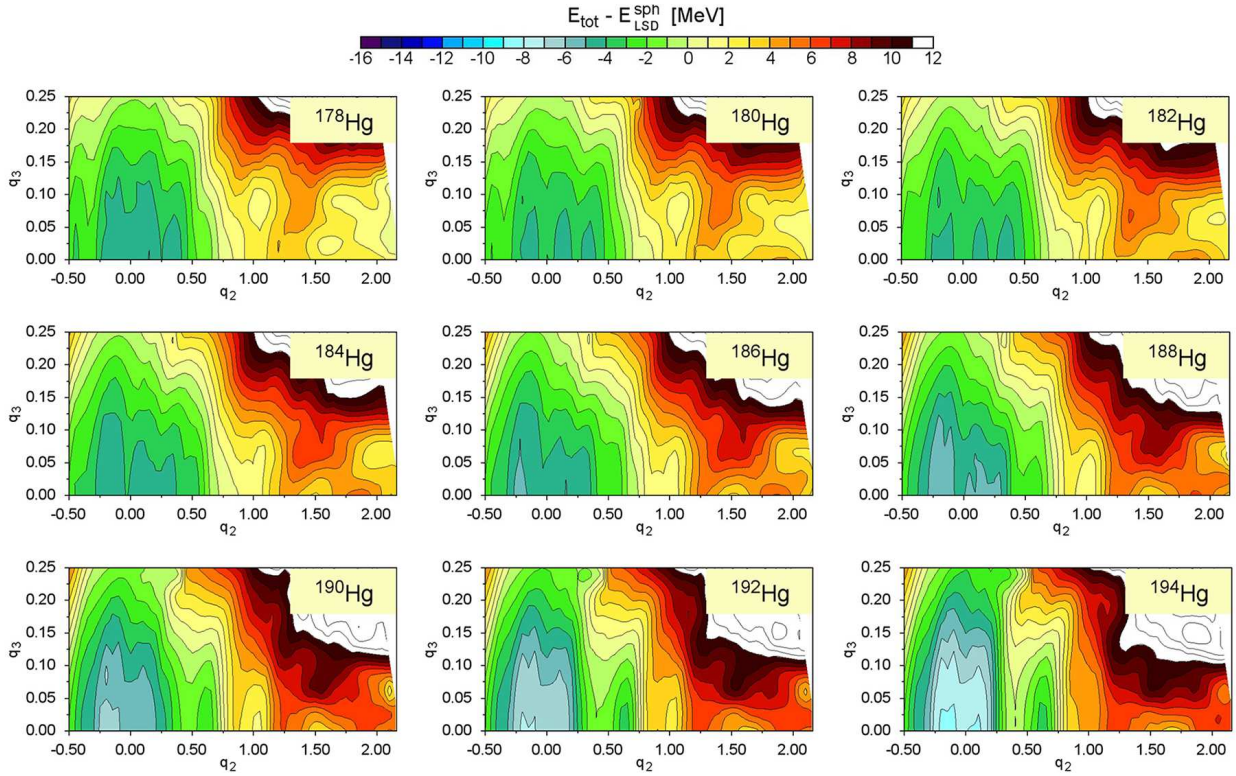

Fig. 7. Same as in fig. 6 but for the Hg isotopes.

q_2 deformation of the sd shape isomers becomes smaller and smaller with increasing neutron number and reaches $q_2 = 0.6$ for ^{194}Hg. As one can conclude from fig. 7, hd shape isomers have a good chance to be observed in $^{184-194}$Hg. The largest ground state quadrupole deformation and a strong competition (coexistence) between prolate and oblate shapes can be observed in $^{182-188}$Hg. As was already noticed in ref. [47], a fission path leading to asymmetric fission is observed in all Hg isotopes, with a heavy-fragment mass between 100 and 110, which is in agreement with the experimental results of Andreyev *et al.* [26].

For the Pb isotopic chain shown in fig. 8, the $Z = 82$ magic number leads to a ground state of zero deformation throughout the chain. Shape isomers corresponding to an elongation $q_2 \approx 0.6$ have a good chance to be found in Pb isotopes with mass number $A = 192$–208. Pronounced hyper-deformed minima are found at $q_2 \approx 1.75$ in the PES of $^{192-204}$Pb, whereas sd shape isomers (with $q_2 \approx 1.3$) are only visible in the heaviest four Pb isotopes $^{202-208}$Pb. All candidates for Pb shape isomers are reflection symmetric ($q_3 = 0$). In heavier Pb isotopes with $A \geq 202$ the previously present mass asymmetric fission path disappears.

It is worth mentioning in this regard that the PES of some of these Pb isotopes is often very *rich*, showing several shape isomeric states on the oblate, but more often on the prolate side. This is in particular the case for the neutron-deficient isotopes between $A = 180$ and $A = 190$. The triple shape coexistence in ^{186}Pb advocated in ref. [49], turns out, according to us, to be a quadruple shape coexistence with two prolate local minima at $q_2 \approx 0.35$ and $q_2 \approx 0.5$ respectively, as shown in fig. 9. Similarly to Andreyev [49], we find the coexistence of an oblate and a prolate minimum at the energies very close to the measured ones. In addition, we have found a second prolate minimum that appears at an only slightly lower energy than two other shape isomeric states. What is shown in fig. 9 is a one-dimensional cross-section of the PES of ^{186}Pb (energy as a function of the only quadrupole q_2 parameter), where, in addition, horizontal lines indicate the position of the ground state and both the excited 0^+ states observed in ref. [49]. Andreyev *et al.* have also observed a rotational band running from the 2^+ to the 14^+ state, and which decays by gamma emission and e^- conversion directly to the 0^+ ground state, while the bottom of this band was not directly observed in ref. [49]. Using the rotational model [50] we have estimated the position of the (non-observed) 0^+ state at which the band ends, and have found it located at approximately 606 keV (dotted line in fig. 9). This value differs from the energies of both 0^+ reported in ref. [49]. This fact can be used as certain confirmation of quadruple shape coexistence in ^{186}Pb. We have found a similar kind of coexistence for other neutron-deficient Pb isotopes, as can be seen from fig. 8.

In the Po isotopic chain analysed in fig. 10, already investigated for some aspects in refs. [46,47], the situation is quite similar to the above described Pb nuclei. Very pronounced sd minima at $q_2 \approx 0.6$ are visible in all isotopes,

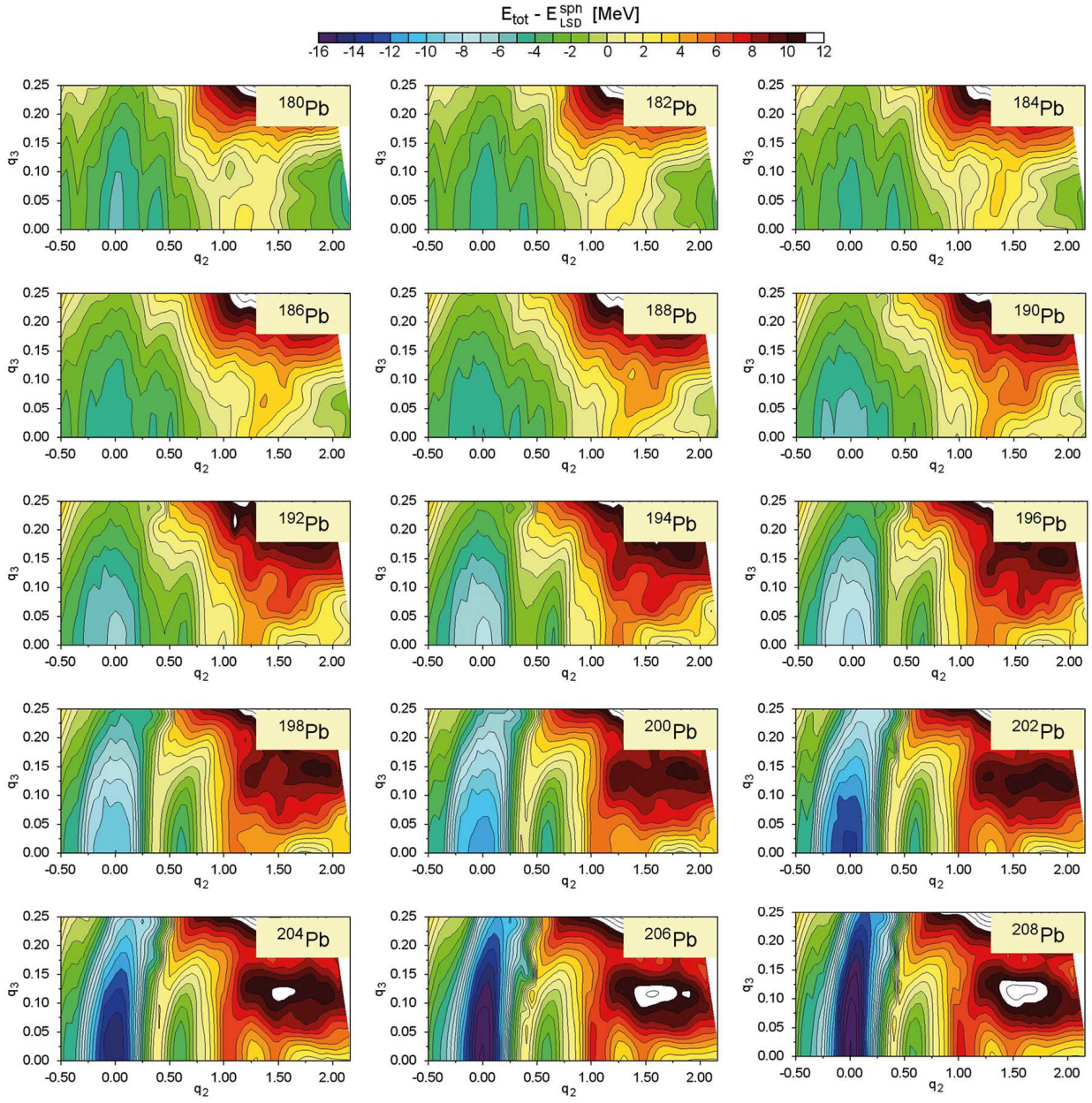

Fig. 8. Same as in fig. 6 but for the Pb isotopes.

except for ^{194}Po. A chance for finding hd shape isomers should exist for Po isotopes with $A \geq 204$. A symmetric and an asymmetric fission path are found only in the most neutron-deficient isotopes, but only a symmetric path is observed for heavier Po nuclei, which is in line with recent experimental data of Ghys and co-workers [51].

The PESs for the chain of Rn isotopes with $A = 196$ to 212 are presented in fig. 11. The ground state of the lightest isotopes corresponds to an oblate shape, while between ^{200}Rn and ^{206}Rn a coexistence between oblate and prolate minima is observed. Starting from $A = 208$ all Rn isotopes are found to be spherical. A sd left-right symmetric shape isomer at $q_2 \approx 0.6$ could be found for $A \geq 198$. Shallow minima corresponding to hd isomers might be found in $^{206-212}$Rn. Similarly to the Po isotopic chain, a mass asymmetric path to fission is visible in the lightest Rn isotopes only.

The Ra isotopic chain, presented in fig. 12, already studied for some aspects in ref. [47] shows a reflection-symmetric path to fission for all the lighter isotopes. An asymmetric path appears with increasing mass number $A \geq 218$ and becomes deeper than the symmetric one for heavier Ra isotopes ($A \geq 224$) in good agreement with the experimental data (see [52] and references therein). The ground state of all light isotopes up to $A = 216$ is found to be spherical. A pronounced octupole deformation

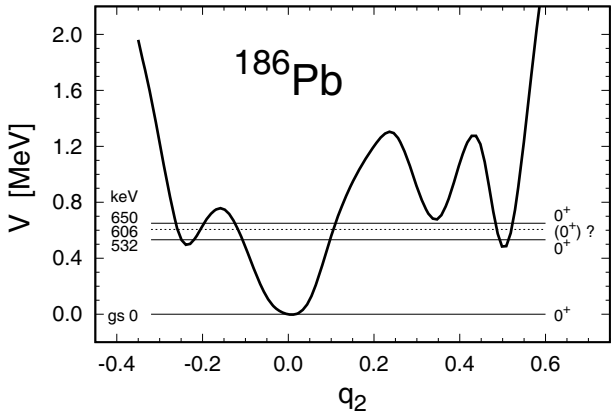

Fig. 9. Potential energy of ^{186}Pb minimized with respect the deformations q_3 and q_4 as function of the elongation parameter q_2. The horizontal (thin solid) lines show the position of the ground and the excited 0^+ states [49], while the dashed line corresponds to the position of the 0^+ rotational band head which we have deduced from the rotational series observed in [49].

($q_3 \neq 0$) appears in the ground state of $^{218-224}$Ra, which is in addition very stiff with respect to truncation of the reflectional symmetry while the quadrupole deformation is around $q_2 \approx 0.25$. These results are in line with the observations made in refs. [53,54] and are also in good agreement with the more recent self-consistent mean-field calculations [55] for ^{224}Ra using the Gogny D1M force. Left-right symmetric sd minima are visible in all Ra isotopes presented here at an elongation q_2 ranging from 0.6 for the lightest to 0.75 for the heaviest nuclei. The large depth of these minima (up to 3 MeV) gives some hope that such shape isomers will be found soon in the experiment. Tiny hd minima can be seen in the PES of $^{228-234}$Ra nuclei at $q_2 \approx 1.2$ and $q_3 \approx 0.1$.

In addition to the above presented isotopic chains, one has to mention that the very deformed shallow minima that we found in the heavier Th and U region [47] are in agreement with calculations using both the macroscopic-microscopic and the self-consistent mean-field models [16,17,25].

The stability of a shape isomer does not only depend on its position in deformation space, but also on the depth of the local minimum. One can assume that shape isomers with a potential well of a depth smaller that 0.5 MeV will be rather difficult to identify in the experiment. Another factor, important for experimentalists, is how high such a local minimum would be located above the ground state. That is why in fig. 13 we present, for all here investigated nuclei, the energies of these local minima numbered by increasing enegy (label 2, 3, ...) corresponding to the ground state (label 1). Nuclei in shape isomeric states could be oblate or prolate deformed reaching, in some cases, super- or even hyper-deformed shapes. Each shape isomeric state is represented in fig. 13 by an ellipse, the length of which reflects the quadrupole deformation in that state (a spherical shape corresponding to a circle). One can notice in fig. 13 that for the Ra isotopic chain there is a sudden drop in energy of the hd isomeric state when the neutron number is increased beyond $N = 132$ ($A = 220$). One could think that such a transition might have to do with some deformed shell closure.

4 Electric quadrupole moments

One possibility to check the quality of our predictions on the deformation of stationary states (gs and shape isomers) is given by the electric quadrupole moment. We have therefore evaluated this quantity within our approach relying on our new Fourier shape parametrization. The results obtained in our model are presented in fig. 14 by the ellipses for each of the isotopic chains between Pt and Ra with negative Q_{20} for the oblate and positive Q_{20} for the prolate shape isomers. Each ellipse in fig. 14 has the same label as the corresponding state in fig. 13. The states with the quadrupole moment larger than 80 eb (*i.e.* for ultra-deformed isomers) visible in some PESs (figs. 6–8, 10–12) are not shown here. Where available, our predictions are compared with the experimental data [56,54]. Usually in experiments one obtains the absolute value of the quadrupole moment, that is why we have put the experimental data with two signs: plus (filled squares) and minus (empty squares). According to our calculation (see fig. 12) the Ra isotopes from $A = 216$ to $A = 228$ are soft with respect to the reflection asymmetric deformation q_3 but stable octupole deformations should appear in Ra isotopes with $218 \leq A \leq 224$ only. This result is in line (but shifted by 2 mass units) with the observation made by Gaffney *et al.* [54], who presented non-zero experimental values for Q_{30} for ^{224}Ra and ^{226}Ra isotopes. Looking at these data one has to bear in mind that the absence of a stable non-zero deformation does not mean that the corresponding electric moment is equal to zero. The role of dynamical effects could be significant when the stiffness related to this mode is small [57]. For example small quadrupole moments measured in some Pb isotopes (see red squares in fig. 14) are due to such dynamical effects. So, the non-zero value of Q_{30} in ^{226}Ra can be obtained after performing a dynamical calculation like done in ref. [57].

The agreement of our results with the data in the ground state is good. Experimental efforts to measure this quantity in the sd and hd region are therefore very strongly encouraged. There is a hope that some of the hd shape isomers could be found in the experiment using, *e.g.*, proton beams that allow to produce compound nuclear systems with not too large angular momentum.

5 Summary

Our investigations on the liquid-drop fission barrier heights and shapes, performed in a variational approach [36], had shown that fission barriers of medium-heavy nuclei are very broad and decrease only slowly when going from saddle to scission. This property of the macroscopic energy offers a chance that in this region of nuclei shell effects might produce local minima at a large nuclear

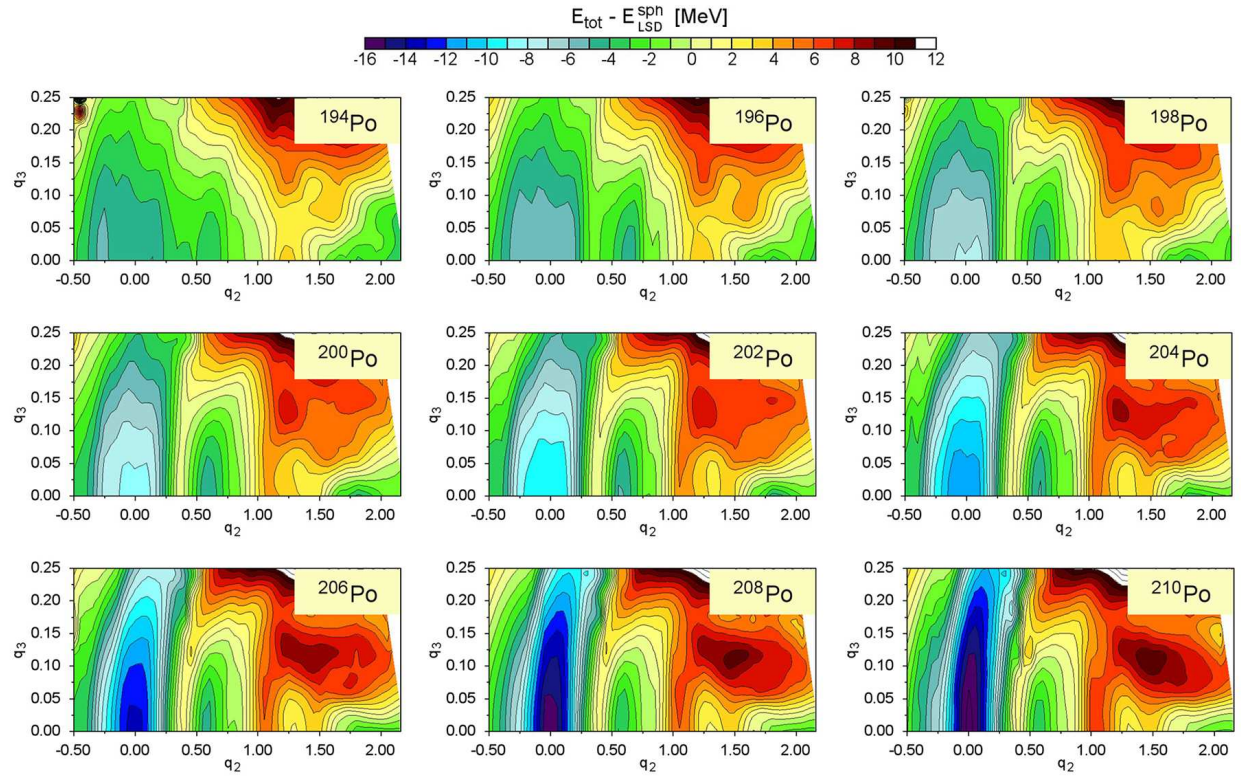

Fig. 10. Same as in fig. 6 but for the Po isotopes.

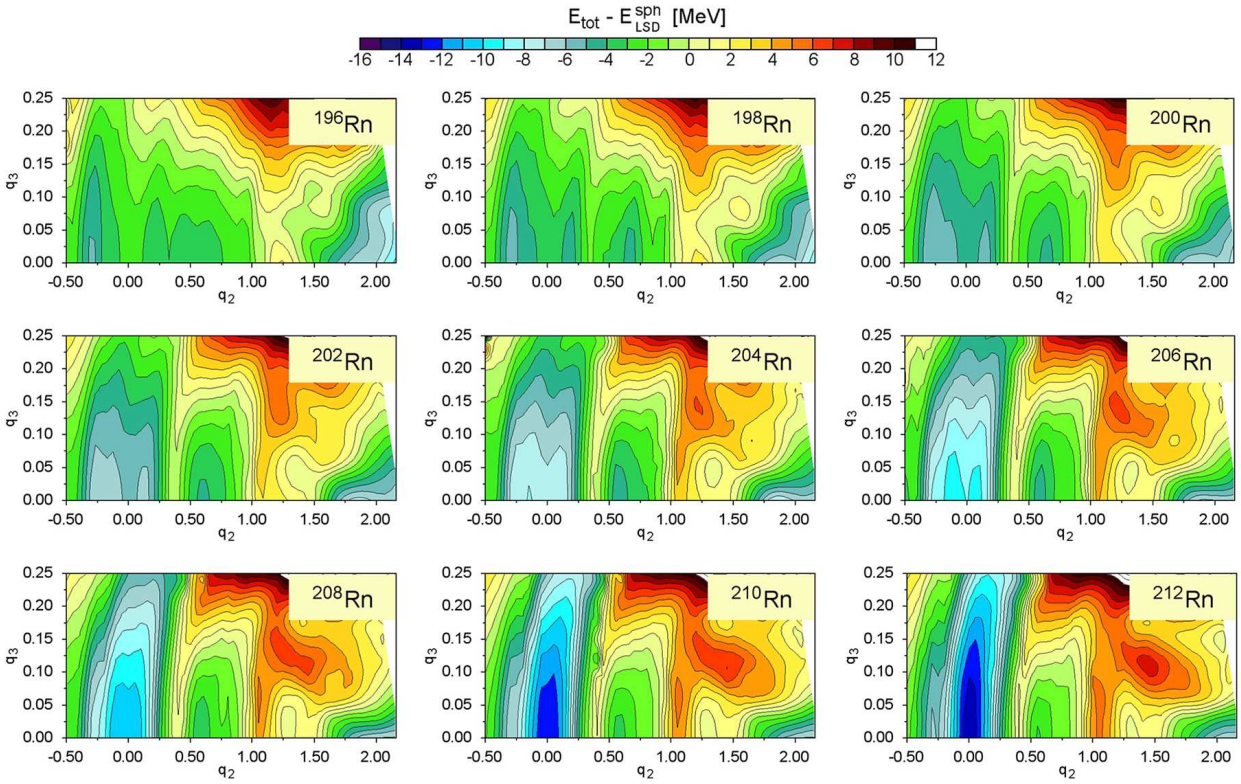

Fig. 11. Same as in fig. 6 but for the Rn isotopes.

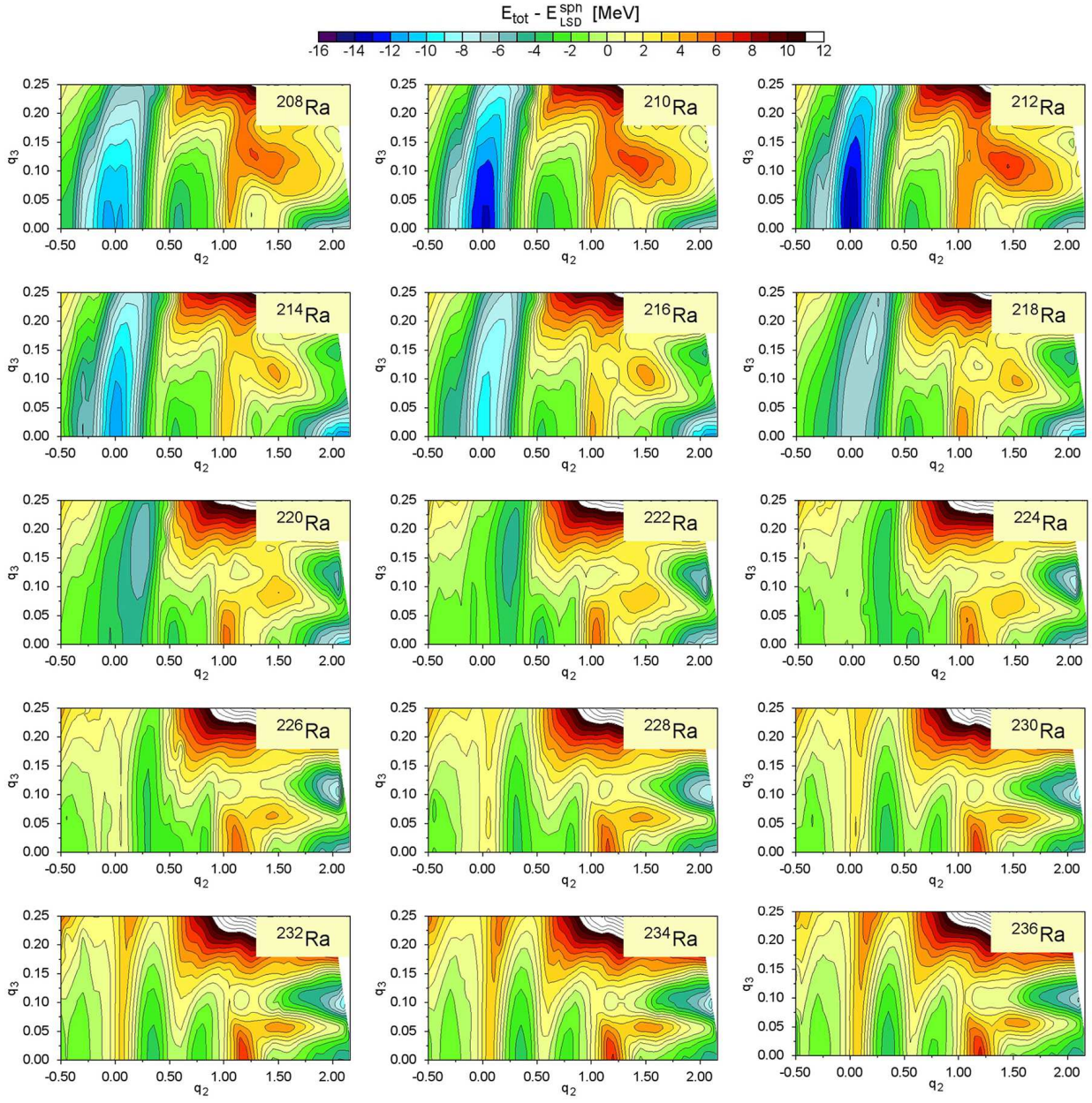

Fig. 12. Same as in fig. 6 but for the Ra isotopes.

elongation. As first candidates, we have chosen the isotopic chains of nuclei between platinum and radium and have shown that the microscopic energy corrections can, indeed, produce pronounced minima in the rather flat macroscopic potential-energy surfaces in this mass region. We have evaluated not only the deformations corresponding to these potential shape isomers but also their height above the ground state and the electric quadrupole moment for all isomeric states as well as for the ground state. The estimates reproduce well the experimental data where available. One has to bear in mind that our static calculation can reproduce the quadrupole moment only in the case of well-deformed nuclei. In transitional nuclei, where the potential energy around the ground state minimum is very flat, like observed in our calculations in the heaviest Pt nuclei or in ^{184,186}Hg isotopes, dynamical effects can increase the magnitude of the quadrupole moment (see ref. [57]). A large $B(E2)$ transition probability corresponding to an electric quadrupole moment could be a fingerprint for super-deformed isomers. We hope that in the near future this new island of super- and hyper-deformed shape isomers will be discovered in the experimental analysis.

One of our next goals is to study the stability of these super- and hyper-deformed shape isomers with respect to fission and light-particle evaporation. For this purpose we are going to use the theoretical models described in refs. [58–60]. We ar also planning to evaluate the rotational bands, that might appear in the nd, sd and hd minima,

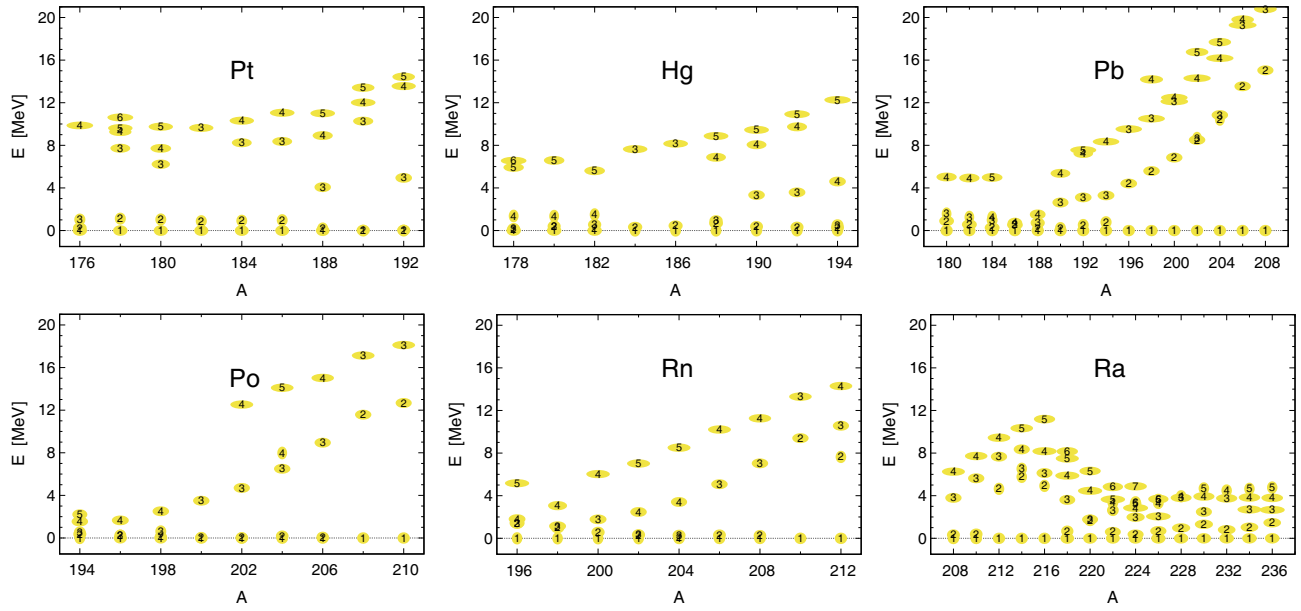

Fig. 13. Energies ground state (label 1) and shape isomeric minima (labels 2, 3, ...) for isotopic chains ranging from Pt to Ra. Each label is surrounded by an ellipse the length of which corresponds to the elongation of the nucleus in that given state.

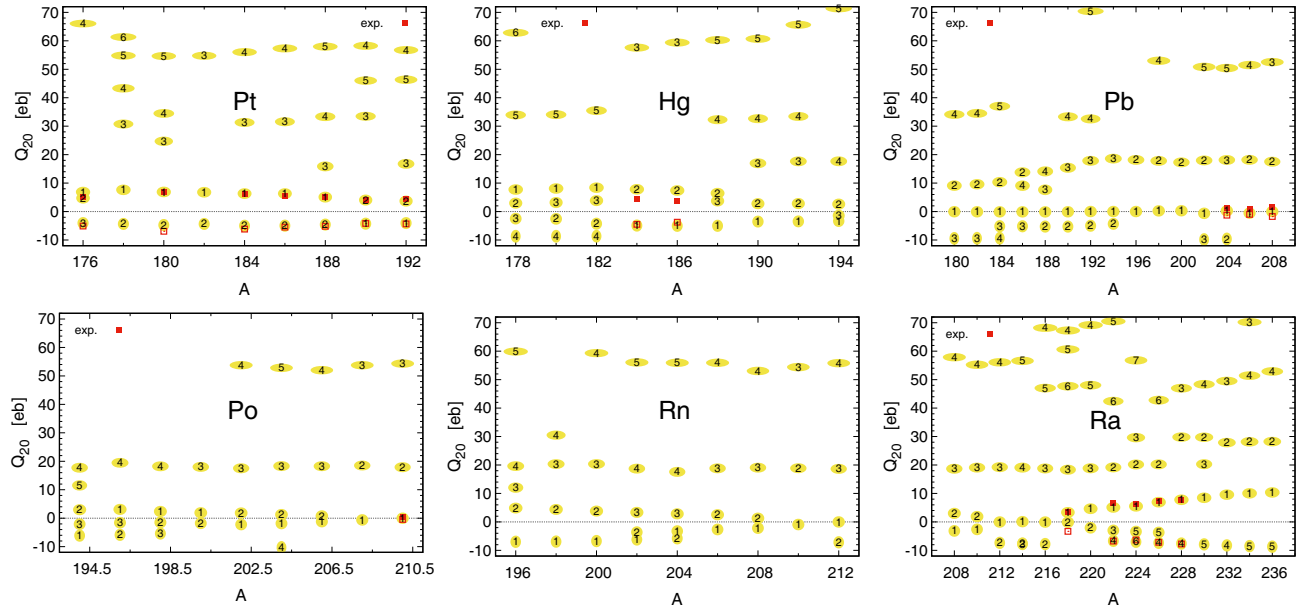

Fig. 14. Electric quadrupole moments (ellipses) obtained in our approach for the ground and the shape isomeric states for isotopic chains between Pt and Ra, with a comparison with available experimental data (boxes) [56,54]. Same labels in figs. 13 and 14 correspond to the same state for each nucleus.

by using the cranking model, like in ref. [61], but taking into account the coupling with the collective pairing and stretching modes [50].

This work has been partly supported by the Polish-French COPIN-IN2P3 collaboration agreement under project number 08-131 and by the Polish National Science Centre, grant No. 2013/11/B/ST2/04087.

References

1. S.M. Polikanov, V.D. Druin, V.A. Karnaukov, V.L. Mikheev, A.A. Pleve, N.K. Skobelev, V.G. Subbotin, G.M. Ter-Akopjan, V.A. Fomichev, Sov. Phys. JETP **15**, 1016 (1962).

2. V.M. Strutinsky, Yad. Fiz. **3**, 614 (1966) Nucl. Phys. A **95**, 420 (1967).
3. W.D. Myers, W.J. Świątecki, Nucl. Phys. **81**, 1 (1966).
4. J. Blons, C. Mazur, D. Paya, Phys. Rev. Lett. **35**, 1749 (1975).
5. J. Blons, C. Mazur, D. Paya, M. Ribrag, H. Weigmann, Nucl. Phys. A **414**, 1 (1984).
6. J. Blons, B. Fabbre, C. Mazur, D. Paya, M. Ribrag, Y. Petin, Nucl. Phys. A **477**, 231 (1988).
7. J. Blons, Nucl. Phys. A **502**, 121c (1989).
8. J.W. Knowles *et al.*, Phys. Lett. B **116**, 315 (1982).
9. M.L. Yoneama *et al.*, Nucl. Phys. A **604**, 263 (1996).
10. A. Krasznahorkay *et al.*, Phys. Rev. Lett. **80**, 2073 (1998).
11. L. Csige *et al.*, Acta Phys. Pol. B **38**, 1503 (2007).
12. L. Csige *et al.*, Phys. Rev. C **80**, 011301(R) (2009).
13. P.G. Thirolf, D. Habs, Prog. Part. Nucl. Phys. **49**, 325 (2002).
14. P. Moller, A.J. Sierk, R. Bengtson, H. Sagawa, T. Ichikawa, At. Data Nucl. Data Tables **98**, 149 (2012).
15. K.T.R. Davies, J.R. Nix, Phys. Rev. C **14**, 1977 (1976).
16. T. Ichikawa, P. Moller, A.J. Sierky, Phys. Rev. C **87**, 054326 (2013).
17. M. Kowal, J. Skalski, Phys. Rev. C **85**, 061302(R) (2012).
18. H.J. Krappe, J.R. Nix, A.J. Sierk, Phys. Rev. C **20**, 992 (1979).
19. K. Pomorski, J. Dudek, Phys. Rev. C **67**, 044316 (2003).
20. S. Ćwiok, W. Nazarewicz, J.X. Saladin, W. Płóciennik, A. Johnson, Phys. Lett. B **322**, 304 (1994).
21. J.F. Berger, M. Girot, D. Gogny, Nucl. Phys. A **502**, 85c (1989).
22. J.-P. Delaroche, M. Girot, H. Goutte, J. Libert, Nucl. Phys. A **771**, 103 (2006).
23. L. Bonneau, P. Quentin, Samsoen, Eur. Phys. J. A **21**, 391 (2004).
24. J. Bartel, P. Quentin, M. Brack, C. Guet, H.-B. Håkansson, Nucl. Phys. A **386**, 79 (1982).
25. J.D. McDonnell, W. Nazarewicz, J.A. Sheikh, Phys. Rev. C **87**, 054327 (2013).
26. A.N. Andreyev *et al.*, Phys. Rev. Lett. **105**, 252502 (2010).
27. M. Warda, A. Staszczak, L. Prochniak, Int. J. Mod. Phys. E **19**, 787 (2010).
28. M. Warda, A. Staszczak, W. Nazarewicz, Phys. Rev. C **86**, 024601 (2012).
29. S. Panebianco, J.-L. Sida, H. Goutte, J.-F. Lemaitre, N. Dubray, S. Hilaire, Phys. Rev. C **86**, 064601 (2012).
30. T. Ichikawa, A. Iwamoto, P. Moller, A.J. Sierk, Phys. Rev. C **86**, 024610 (2012).
31. A.V. Andreev, G.G. Adamian, N.V. Antonenko, A.N. Andreyev, Phys. Rev. C **88**, 047604 (2013).
32. J.D. McDonnell, W. Nazarewicz, J.A. Sheikh, A. Staszczak, M. Warda, Phys. Rev. C **90**, 021302 (2014).
33. C. Schmitt, B. Nerlo Pomorska, K. Pomorski, J. Bartel, Phys. Rev. C **95**, 034612 (2017).
34. K. Pomorski, J. Dudek, Int. J. Mod. Phys. E **13**, 107 (2004).
35. W.D. Myers, W.J. Świątecki, Nucl. Phys. A **612**, 249 (1997).
36. F.A. Ivanyuk, K. Pomorski, Phys. Rev. C **79**, 054327 (2009).
37. K. Pomorski, B. Nerlo Pomorska, J. Bartel, C. Schmitt, Acta Phys. Pol. B Suppl. **8**, 667 (2015).
38. A. Dobrowolski, K. Pomorski, J. Bartel, Comp. Phys. Commun. **199**, 118 (2016).
39. M. Brack, J. Damgaard, A.S. Jensen, H.C. Pauli, V.M. Strutinsky, C.Y. Wong, Rev. Mod. Phys. **44**, 320 (1972).
40. S.G. Nilsson *et al.*, Nucl. Phys. A **131**, 1 (1969).
41. A. Góźdź, K. Pomorski, Nucl. Phys. A **451**, 1 (1986).
42. K. Pomorski, Int. J. Mod. Phys. E **16**, 237 (2007).
43. K. Pomorski, J. Bartel, Int. J. Mod. Phys. E **15**, 417 (2006).
44. J. Bartel, A. Dobrowolski, K. Pomorski, Int. J. Mod. Phys. E **16**, 459 (2007).
45. B. Nerlo-Pomorska, K. Pomorski, C. Schmitt, J. Bartel, Phys. Scr. **90**, 114010 (2015).
46. B. Nerlo Pomorska, K. Pomorski, J. Bartel, Acta Phys. Pol. B **47**, 943 (2016).
47. B. Nerlo Pomorska, K. Pomorski, J. Bartel, C. Schmitt, Acta Phys. Pol. B Suppl. **10**, 173 (2017).
48. B. Nerlo Pomorska, K. Pomorski, J. Bartel, C. Schmitt, to be published in Acta Phys. Pol. B **48** (2017).
49. A.N. Andreyev *et al.*, Nature **405**, 430 (2000).
50. B. Nerlo-Pomorska, K. Pomorski, J. Bartel, Phys. Rev. C **84**, 044310 (2011).
51. L. Ghys *et al.*, Phys. Rev. C **90**, 041301(R) (2013).
52. K.-H. Schmidt *et al.*, Nucl. Phys. A **665**, 221 (2000).
53. P.A. Butler, W. Nazarewicz, Rev. Mod. Phys. **68**, 349 (1996).
54. L.P. Gaffnery *et al.*, Nature **497**, 199 (2013).
55. L.M. Robledo, P.A. Butler, Phys. Rev. C **88**, 051302 (2013).
56. S. Raman, C.W. Nestor Jr., P. Tikkanen, At. Data Nucl. Data Tables **78**, 1 (2001).
57. B. Nerlo-Pomorska, K. Pomorski, Z. Phys. A **309**, 341 (1983).
58. J. Randrup, S.E. Larsson, P. Moller, S.G. Nilsson, K. Pomorski, A. Sobiczewski, Phys. Rev. C **13**, 229 (1976).
59. A. Zdeb, M. Warda, K. Pomorski, Phys. Rev. C **87**, 024308 (2013).
60. K. Pomorski, M. Warda, A. Zdeb, Phys. Scr. **90**, 114013 (2015).
61. A. Sobiczewski, S. Bjornholm, K. Pomorski, Nucl. Phys. A **202**, 274 (1973).